Title

Ionic Conductive and Highly-Stable Interface for Alkali Metal Anodes

Journal

Small, 18(33)

ISSN

1613-6810

Authors

Jin, Enzhong

Tantratian, Karnpiwat

Zhao, Changtai

et al.

Publication Date

2022-08-01

DOI

10.1002/smll.202203045

Ionic Conductive and Highly-Stable Interface for Alkali Metal Anode

Enzhong Jin[1+], Karnpiwat Tantratian[2+], Changtai Zhao[1], Anastasia Codirenzi[4], Lyudmila V. Goncharova[4], Changhong Wang[1], Feipeng Yang[3], Parham Pirayesh[1], Jinghua Guo[3], Lei Chen[2, 5], Xueliang Sun[1*], Yang Zhao[1*]*

[1]Department of Mechanical and Materials Engineering
University of Western Ontario, London, Ontario, N6A 5B9, Canada
Email: X. Sun: xsun9@uwo.ca; Y. Zhao: yzhao628@uwo.ca

[2]Department of Mechanical Engineering
University of Michigan–Dearborn, Dearborn, Michigan 48128, United States
Email: L. Chen: leichn@umich.edu

[3]Advanced Light Source
Lawrence Berkeley National Laboratory, Berkeley, CA, 94720, United States

[4]Department of Physics and Astronomy
University of Western Ontario, London, Ontario, N6A 3K7, Canada

[5]Michigan Institute for Data Science
University of Michigan, Ann Arbor, Michigan 48109, United States

+ These authors contribute equally to this work

Abstract

Alkali metal anodes, such as Li and Na metals, are regarded as the most promising candidates for next-generation batteries due to their high specific capacity, low electrochemical potential, and lightweight. However, critical problems of the state-of-the-art alkali metal anodes, especially dendrite formation and interface stabilization, remain challenging to overcome. The solid electrolyte interphase (SEI) refers to the native complex interphase(s) electrochemically/chemically formed as a thin film on the surface of electrodes against electrolytes. SEI layer is one of the key factors affecting Li and Na deposition behavior and electrochemical performances. In this study, we successfully develop a facile and universal approach to fabricating ionic conductive interfaces for both Li and Na metal anodes by modified atomic layer deposition (ALD). In this process, the Li metal (or Na metal) plays the role of Li (or Na) source without any additional Li (Na) precursor during ALD. Moreover, we address the key questions about ALD deposition temperature's influence on the compositions and structures of the coating. The optimized ionic conductive coatings have significantly improved the electrochemical performances. In addition, the electrochemical phase-field model has been performed to prove that the ionic conductive coating is very effective in promoting uniform electrodeposition. This approach is universal and potentially used for other different metal anodes. At the same time, it can be extended to other types of coatings or other deposition techniques.

1. Introduction

Alkali metal anodes, such as Li and Na metals, with high theoretical capacity, low electrochemical potential, and lightweight, are considered as one of the most promising candidates for the next-generation alkali-metal batteries, including Li/Na-S, Li/Na-O_2, and all-solid-state Li/Na metal batteries[1-5]. However, several serious challenges exist for alkali metal anodes, limiting their practical applications. The dendrite growth is one of the major challenges, which leads to undesired safety concerns, low Coulombic efficiency (CE) and inactive ""dead Li/Na"" layer formation[6-7]. The solid electrolyte interphase (SEI) layer, naturally formed due to the chemical/electrochemical reaction between alkali metal and electrolyte, is critical for the electrochemical deposition behaviour and electrochemical performances of the alkali metal anode, in which the structure, composition, and stability of the SEI layer are key factors[8-9]. The unstable SEI layer can promote dendrite growth due to the nonuniform ion flux distribution and non-homogeneous alkali metal depositions, leading to the large polarization and the decay of the 'batteries' performances[10-11]. Tremendous efforts have been attempted to stabilize the SEI via different approaches, including modifying the electrolyte components and creating artificial SEI layers for alkali metal anode. The artificial SEI layers are expected to block the side reactions between electrolyte and alkali metal, stabilize the interface, reduce the dendrite growth, and improve performances[12-13]. Many protective layers have been developed for both Li and Na metal anodes, including inorganic layers, organic layers, and organic-inorganic hybrid layers[14-19].

Generally, an ideal artificial SEI layer should possess the properties of ultrathin thickness, uniform and complete coating, high ionic conductivity, sufficient density, and good mechanical stability. The fabrication of the ideal artificial SEI layer that can meet all these requirements is a challenge. Atomic layer deposition (ALD) is a unique technique to design the surfaces and interfaces of alkali metal anode at the atomic scale with excellent coverage and conformal deposition characteristics under relatively low temperatures with precise control over coating thicknesses[20-21]. In the reported literature, several types of films have been fabricated as protective layers for both Li and Na metal anodes by ALD, such as metal oxide, polymers, and hybrid films[22-28]. The ultra-thin protective layers by ALD can effectively reduce the dendrite formation and significantly enhance the electrochemical/chemical stability. Although impressive progress has been achieved with ALD-protected alkali metals, challenges remain. Firstly, most

of the developed ALD coatings for alkali metals are non-ionic conductive and had to be lithiated/ sodiated during the electrochemical plating/stripping process. The initial lithiation/sodiation steps may cause the non-homogeneous Li/Na depositions on the surface of Li metal. The major limitation to deposit ionic conductive layer on Li/Na metal by ALD is the high deposition temperature (over 200 °C) and high precursor temperature (over 180 °C), which is above the melting point of the alkali metals, such as Li (180.5 °C) and Na metals (97.8 °C)[29-30]. Secondly, although some studies reported the ALD metal oxides for Li or Na protection, the influences of the deposition temperature in the ALD process have not been studied. Thirdly, the chemical composition and micromechanism of metal oxide and solid-state electrolyte as artificial SEI 'have not been comprehensively understood.

Herein, we propose a universal approach to fabricate ion-conductive coatings for the alkali metal anodes (Li and Na metal as examples) by ALD. In this process, a two-step strategy is developed to obtain the smooth and stable $LiAlO_x$ and $NaAlO_x$ artificial layer for Li and Na metal anodes by the post lithiation process, respectively. Remarkably, the coating layers are successfully achieved on the surface of metals with excellent quality and significantly improved performances. In addition, we have studied the ALD deposition temperature effects on the structures of the protective layers and electrochemical performances. The surface and interface chemistry and Li deposition behaviors have been deeply studied by different advanced characteristic techniques. Moreover, the electrochemical phase-field model has been performed to reveal how beneficial the ionic conductive coating is in promoting uniform electrodeposition. On one hand, our design of the ionic conductive protective layer for highly stable alkali metal anodes may open the new window to creating conductive layers on Li and Na metal, which can be extended to other ALD materials or other thin film deposition techniques. On the other hand, this study provides new insight into the temperature effects of Li and Na metal as a substrate during the ALD deposition process.

2. Results and Discussion

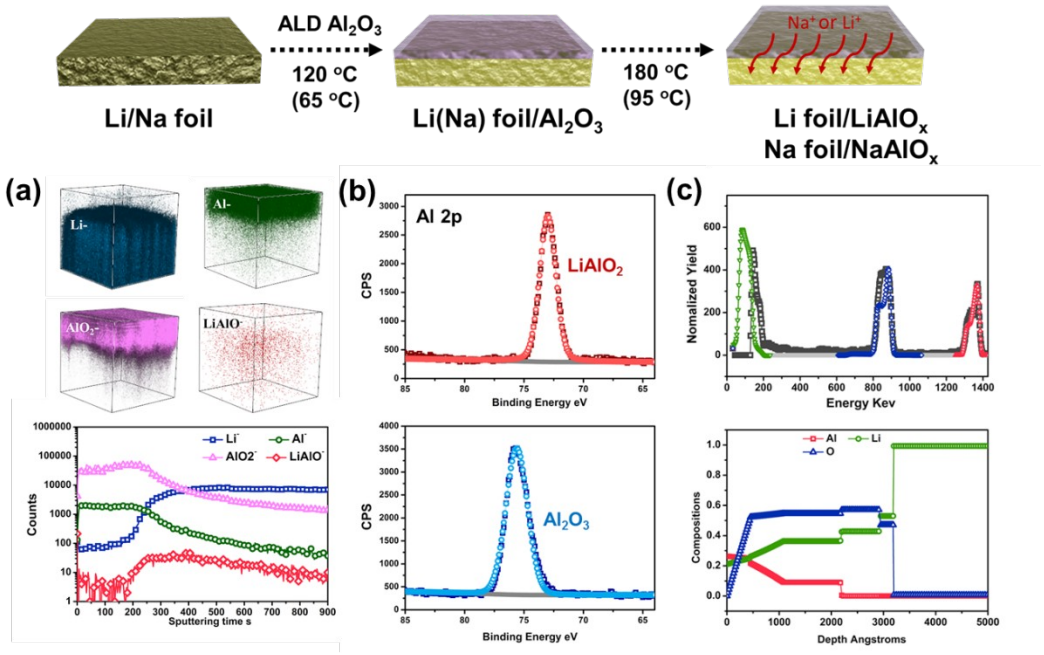

Fig.1 (a) Schematic diagram of the two-step strategy to fabricate the ionic conductive layers on Li or Na metal anodes; (b) XPS spectrum of Al 2p of Li@200Al_2O_3 and Li@200$LiAlO_x$-ex; (c) TOF-SIMS secondary ion images, depth profile of various secondary ion species and corresponding 3D images of Li@200$LiAlO_x$-ex; (d) RBS spectra and calculated depth profiles of Li@200$LiAlO_x$-ex.

The ALD metal oxides have been proven effective artificial SEI for Li metal anode previously. The deposition temperatures of the reported ALD metal oxides are generally below 150 °C. Two important questions remain in this area. Firstly, is it possible to synthesize the lithiated layers on Li metal by ALD without the introduction of an extra Li precursor? Secondly, does the ALD deposition temperature affect the structures or compositions of the coatings? To address these questions, we designed the experiments by controlling the ALD deposition temperatures and developed a new two-step strategy. We first studied the ALD deposition temperature effects for Li metal anodes. The ALD Al_2O_3 was used for demonstration because it is the most popular and effective coating for battery interface modification. The deposition temperature of ALD Al_2O_3 was controlled at 120 °C (below the melting point of Li) and 180 °C (over the melting point of Li), in which the samples are named as Li@nAl_2O_3 and Li@n$LiAlO_x$-in (n=ALD cycles), respectively. Furthermore, the two-step approach was developed, as shown

in the schematic diagram in **Fig. 1(a)**. In this two-step approach, the ALD Al_2O_3 was first deposited on Li metal at the regular temperature of 120 °C. Then, the ALD chamber was heated up to 180 °C for the post-treatment and kept for half an hour. The samples obtained by this ex-situ process are named as Li@n$LiAlO_x$-ex (n=ALD cycles). This approach can be extended to other metal anodes (such as Na metal anode) and other coating layers. For example, the ALD Al_2O_3 is firstly deposited on the Na metal anode at relatively low temperatures (65 °C) and then post sodiation process is carried out at the temperature close to the melting point of Na metal (97.8 °C).

X-ray photoelectron spectroscopy (XPS) was used to investigate the surface of Li foil after Al_2O_3 deposition under different conditions, which are shown in **Fig. 1(b)** and **Fig. S1-3**. From the full spectrum presented in **Fig. S1-3**, Peaks around 75 eV and 532 eV are attributed to Al and O, respectively. It is demonstrated that the Al_2O_3 contained films have been successfully deposited on the Li foils. **Fig. 1(b)** shows the detailed spectrum of Al 2p for Li@200Al_2O_3 and Li@200$LiAlO_x$-ex. For the Li@200Al_2O_3 deposited at 120 °C, the peak of Al 2p at 75.6 eV represents the typical chemical state with Al_2O_3 reported in the literature After post-annealing above the melting point for Li@200$LiAlO_x$-ex, the peak of Al 2p slightly shifts to the low binding energy of 72.9 eV, indicating the successful reaction and lithiation between Li metal and Al_2O_3 to form the $LiAlO_x$. As shown in **Fig. S3**, the peak of Al 2p for Li@$LiAlO_x$-in is also at 75.6 eV, demonstrating the similar $LiAlO_x$ film formed on the Li surface during the high-temperature ALD deposition process. The soft X-ray Absorption Spectroscopy Near-Edge Structure (XASNES) at Al K edge was carried out to further elaborate on the compositions of the designed samples, as shown in **Fig. S4**. For the standard Al_2O_3 powder sample, the main peak at 1564.7 eV is assigned to transitions from the Al 1s orbitals into Al 3p and O 2p antibonding orbitals of t_{1u} symmetry. In the spectra of $LiAlO_2$ powder, this main peak slightly shifts to the low energy of 1563.6 eV. Compared to the Li@200Al_2O_3, the pre-edge and main peak features of Li@200$LiAlO_x$-ex and Li@200$LiAlO_x$-in also shift to the lower energy, indicating the lithiation of the films causing the observed change in the local electronic structures of Al. Based on the XPS and XAS results, it can be concluded that both the high-temperature ALD and post-annealing processes can lead to the lithiation of Al_2O_3 to form $LiAlO_x$ on the surface of Li foils. Moreover, the X-ray Diffraction (XRD) patterns of Li@200Al_2O_3, Li@200$LiAlO_x$-ex, and

Li@200LiAlO$_x$-in are shown in **Fig. S5**. From the XRD results, it can be seen that all the films on Li metal are amorphous without any peaks related to Al_2O_3 or $LiAlO_2$.

To probe the thicknesses and chemical compositions of the deposited films, the time-of-flight secondary ion mass spectrometry (TOF-SIMS) and Rutherford backscattering spectrometry (RBS) were performed, as shown in **Fig. 1(c, d)** and **Fig. S6-10**. **Fig. S6 (a)** presents the RBS spectra and simulated depth profile of Li@200Al_2O_3. Al and O peaks from the surface can confirm the successful synthesis of an Al-contained layer on Li metal. The thickness of the Al_2O_3 for Li@200Al_2O_3 is about 50 nm with another mixture interlayer of 60 nm. After annealing at 200 ºC (Li@200LiAlO$_x$-ex), the top surface layer is still around 50 nm and Li content in the top layer significantly increases due to the lithiation process, further confirming the formation of $LiAlO_x$ (As shown in **Fig. 1(c)**). Moreover, the Al also diffuses deeper into the Li foil to form the thicker interlayer of another 100 nm. However, the Li@200LiAlO$_x$-in that deposited at the melting point of Li displays a much thicker layer of $LiAlO_x$ with a thickness above 230 nm, as shown in **Fig. S6(b)**. The Al of Li@200LiAlO$_x$-in permeates quite deep into the Li foil with another 200 nm layer. Moreover, the O spectrum of Li@200LiAlO$_x$-in shows that oxygen penetrates above 1 μm on the surface of Li foil. The Li@200LiAlO$_x$-in was fabricated directly at a high temperature at the melting point of Li metal. In this case, the Li is easier to react with H_2O to form the LiOH and this reaction might cause the continuous corrosion of Li metal to form the thick O-rich interlayer. **Fig. S7** shows the RBS spectra and simulated depth profiles of the Li@LiAlO$_x$-ex with different thicknesses (Li@300LiAlO$_x$-ex and Li@500LiAlO$_x$-ex). The thicknesses increase from ~ 80 nm to ~ 100 nm with an increase in ALD cycles from 300 cycles to 500 cycles. From the RBS results, it can be further confirmed that the Li can diffuse and react with Al_2O_3 to form the $LiAlO_x$ for both Li@200LiAlO$_x$-ex and Li@200LiAlO$_x$-in. However, the in-situ high-temperature ALD process causes the corrosion of Li foil with a thick O-rich interlayer formation. Based on this, the two-'step approach is more promising to form a smooth and thickness controllable $LiAlO_x$ on Li metal anode.

More detailed information is obtained from TOF-SIMS results, as shown in **Fig.1 (c)** and **Fig. S7**. **Fig. 1(c)** presents the top surface secondary ion images of Li^-, AlO^{2-}, and Al^- and their depth profiles and corresponding 3D reconstructed images for Li@200LiAlO$_x$-ex. From the chemical ion images on the surface of Li, it can be observed that the Li foil is uniformly covered

with Al contained films. There is almost no signal of Li- species detected on the top surface. As expected, the signals of $AlO^{2-}$and Al^{-} decrease, whereas the signal of Li^{-} remains constant after 300 s Cs+ sputtering, which is clearly observed from the depth profiles and corresponding 3D reconstructed images. Moreover, there are Li^{-} diffusions into the Al-contained films from the 3D reconstructed image, further proving the lithiation of Al_2O_3. However, it needs to be mentioned that the Li^{-} count is not high because it is the negative ions. Moreover, the interface between the Al-contained layer and Li surface is relatively smooth, indicating that the post-treatment at high temperature does not affect the morphology of the coating layer and Li surface. As a comparison, the depth profiles and corresponding 3D reconstructed images of Li^{-}, AlO^{2-}, LiO^{-} and Al^{-} for Li@200$LiAlO_x$-in are shown in **Fig. S8**. Consistent with the RBS result, the in-situ high-temperature ALD process on Li metal leads to the very thick Al-contained film (sputtering time over 800 s). Moreover, there is a very strong LiO^{-} signal from the top surface penetrating to the bulk Li, demonstrating the corrosion of Li metal by the H_2O precursor. Meanwhile, the deposition of the $LiAlO_x$ film is nonuniform and the interface between Li metal and $LiAlO_x$ is quite rough. The surface morphologies of the different designs were further tested by scanning electron microscope (SEM), as shown in **Fig. S9-10**. From the top view SEM images for Li@200$LiAlO_x$-ex, Li@300$LiAlO_x$-ex, and Li@500$LiAlO_x$-ex, the surfaces of the $LiAlO_x$ protected Li foils are relatively smooth and very similar to the pristine Li foil. However, the surfaces of Li@25$LiAlO_x$-in and Li@100$LiAlO_x$-in are quite rough compared to the two steps post-treated samples, which is consistent with the TOF-SIMS analysis.

A similar two-step approach has been applied for Na metal anode to prove the concept and universality. The ALD Al_2O_3 is firstly deposited on the Na metal anode at 65 ^{o}C (the sample is named as Na@200Al_2O_3) and then the ALD chamber is heated up at 98 ^{o}C) for sodiation process (the sample is named as Na@200$NaAlO_x$). **Fig. S11-12** show the TOF-SIMS results of surface secondary ion images, depth profile, and corresponding 3D images of secondary ion species for Na@200Al_2O_3 and Na@200$NaAlO_x$, respectively. Compared to Na@200Al_2O_3, the Na is successfully diffused into the Al_2O_3 layer to form the NaAlOx with the post-sodiation process for Na@200$NaAlO_x$. The stronger signal from Na secondary ion species in the top coating layer is observed from both depth profile and corresponding 3D images for Na@200$NaAlO_x$. From the SEM images for Na@200Al_2O_3 and Na@200$NaAlO_x$ in **Fig. S13**, it can be observed that the

surface morphology and structure of the coating layer are not changed with post sodiation process at melting temperature. The results prove that this two-step approach is universal for fabricating ionic conductive coating layers for alkali metal anodes.

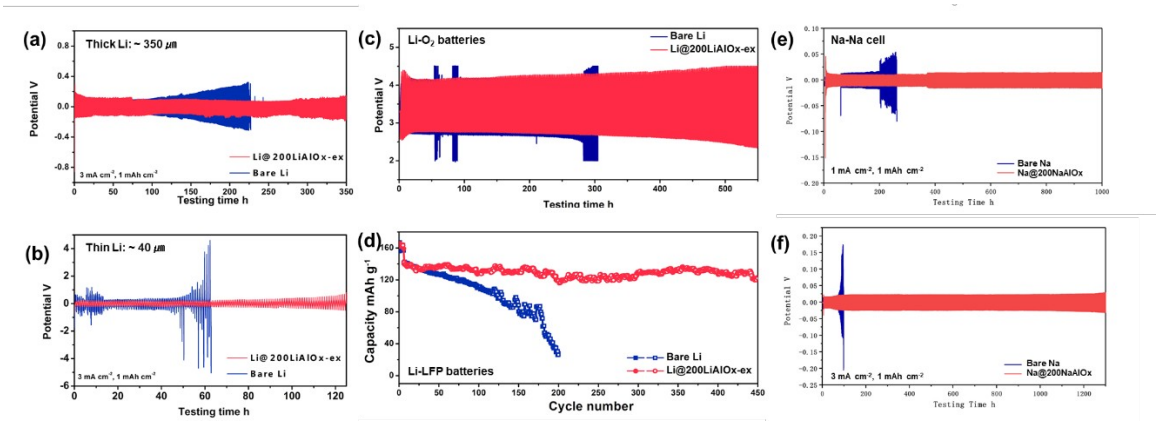

Fig.2 The overpotentail of Li/Li symmetric cells using bare Li foil and Li@200LiAlO$_x$-ex in the carbonate-based electrolyte at the current density of 3 mA cm^{-2} with the capacity of 1 mAh cm^{-2} with (a) thick Li foil (~350 μm) and (b) thin Li foil (~40 μm). (c) Cycling performances of Li-O$_2$ full cells (CP-NCNTs as the cathode) using bare Li foil and Li@200LiAlO$_x$-ex as anode electrode at the current density of 0.1 mA cm^{-2}. (d) Cycling performances of full cells (C/LiFePO$_4$ as the cathode) using bare Li foil and Li@200LiAlO$_x$-ex as anode electrode at 1 C (1C=170 mA g^{-1}). The overpotentail of Na/Na symmetric cells using bare Na foil and Na@200NaAlO$_x$ under the conditions of (e) 1 mA cm^{-2}/1 mAh cm^{-2} and (f) 3 mA cm^{-2}/1 mAh cm^{-2}

Symmetrical cells were assembled to evaluate the Li plating/stripping behavior of the different designs of the coating layers. **Fig. S14** shows the electrochemical performances of the Li@100Al$_2$O$_3$, Li@100LiAlO$_x$-in, and Li@100LiAlO$_x$-ex in the symmetrical cells. At the current density of 1 mA cm^{-2} with the capacity of 1 mAh cm^{-2}, the Li@100Al$_2$O$_3$ displays the over-potential of ~ 200 mV over 400 h. In the reported literature, the thin Al$_2$O$_3$ with few nanometers can improve the cycling performances, however, thick Al$_2$O$_3$ may lead to even worse performance due to ionic insulative Al$_2$O$_3$ with nonuniform Li deposition. The Li@100LiAlO$_x$-in deposited at high temperature presents better performances compared to the Li@100Al$_2$O$_3$ with

the stable over-potential over 600 h. Remarkably, the Li@100$LiAlO_x$-ex shows the best performance of over 800 h among all the samples. After increasing the current density into 5 mA cm^{-2}, the advantage of Li@100$LiAlO_x$-in is not as obvious as at low current density, in which the electrochemical performance of Li@100$LiAlO_x$-in is slightly better than that of the Li@100Al_2O_3. The reason could be that although the Al_2O_3 for Li@100$LiAlO_x$-in was lithiated under the high-temperature ALD, the continuous corrosion of Li metal by H_2O lead to the O-rich interlayer and nonuniform $LiAlO_x$ layer with a rough surface. Promisingly, the Li@100$LiAlO_x$-ex keeps the superiority compared to the other two designs. In this case, it can be concluded that the two-step approach (Li@n$LiAlO_x$-ex) with a post-treatment can be considered as the effective approach to lithiate the Al_2O_3 to form LiAlOx on the Li metal surface with high uniformity and controlled thicknesses. In addition, the thickness of Li@n$LiAlO_x$-ex was further optimized, as shown in **Fig. S15**. Various thicknesses of 50, 100, 150, 300 and 500 cycles of $LiAlO_x$ were deposited on the Li anodes. At different current densities (1 mA cm^{-2} and 3 mA cm^{-2}), the optimized thickness of the $LiAlO_x$ is around 150-300 ALD cycles.

As discussed above, the two-septs approach with post-treatment produces high quality and preciously controlled $LiAlO_x$ coating on the Li surface. In this case, we picked up the Li@200$LiAlO_x$-ex as an example of the 'battery's performance study. **Fig. 2(a)** and **Fig. S16(a)** show the cycling stability of bare Li foil and Li@200$LiAlO_x$-ex at different conditions using conventional Li foil with a thickness of 350 μm. At the current density of 1 mA cm^{-2} with the capacity of 1 mAh cm^{-2}, the initial Li stripping/plating over-potential of bare Li foil is approximately 50 mV (versus Li^+/Li) and rapidly increases to over 200 mV (versus Li^+/Li) after ~ 650 h. Then, the over-potential of bare Li foil keeps over 300 mV and is fluctuant. However, Li@200$LiAlO_x$-ex displays significant improvement in cycling stability. The over-potential of Li@200$LiAlO_x$-ex is stable with a low over-potential of 100 mV after 1000 h without any short circuit. **Fig. S16(a)** displays the symmetrical cell performances of bare Li foil and Li@200$LiAlO_x$-ex at a higher current density of 3 mA cm^{-2}. The bare Li foil still shows the increased over-potential and subsequently short circuit after ~ 225 h. In comparison, the Li@200$LiAlO_x$-ex displays improved stability with a stable overpotential over 350 h. For more practical applications, thin Li foil is requested to obtain high energy density. In this case, we also used the thin Li foil with a thickness of 40 μm. The electrochemical performances of the

symmetrical cell for the bare Li foil and Li@200LiAlO$_x$-ex using thin Li foil are shown in **Fig. 2 (b)** and **Fig. S16 (b)**. In **Fig. S16 (b)**, the over-potential of the bare thin Li foil starts to increase after 200 h and reaches 1000 mV after 225 h, indicating the depletion of the Li metal and formation of dead Li layers. As a comparison, the thin Li@200LiAlO$_x$-ex is stable over ~ 330 h without a short circuit. The bare thin Li foil is extremely unstable at the high current density of 3 mA cm^{-2}, as shown in **Fig. 2(B)**. The lifetime of the bare thin Li foil is less than 50 h. However, the cycling stability of the thin Li@200LiAlO$_x$-ex is over 120 h and about two times higher than that of the thin Li foil. It is also worth mentioning that the electrochemical performances of the thin Li even with coatings are generally worse than the thick Li due to the consumption of Li metal and electrolyte, which has been widely recognized in this field.

In order to further demonstrate the unique properties of the LiAlO$_x$ coating, different full cell systems have been investigated using bare Li foil and Li@LiAlO$_x$-ex electrodes as the anode. Based on the symmetric cell performances discussed above, the Li@200LiAlO$_x$-ex electrode is used as an example for the full cells. The electrochemical performances of the Li-O_2 batteries were performed by using 2016-type coin cells of a carbon-based cathode (N-doped carbon nanotube grown on carbon paper, NCNTs-CP), an electrolyte of $LiClO_4$ in tetraethylene glycol dimethyl ether (TEGDME) and a bare Li foil or protected Li foil (Li@200LiAlOx-ex) as the anodes. **Fig. 2 (c)** and **Fig.S17** present the charge-discharge profiles and cycling performances of the Li-O_2 cells using bare Li foil and Li@200LiAlOx-ex as anodes, respectively. For the bare Li anode, the performance of the Li-O_2 cell is less than 280 h (140 cycles). However, the protected Li of Li@200LiAlOx-ex delivers a significantly improved cycling stability of ~ 550 h (300 cycles), which is two times higher than that of the cell using a bare Li anode. The results reveal that the LiAlOx coating can effectively reduce the degradation of Li anodes against O_2 corrosion and Li dendrite formation. Furthermore, the Li-$LiFePO_4$ (LFP) batteries were demonstrated in **Fig. 2 (d).** The LFP cells were firstly activated at 0.1 C for 5 cycles and then cycled at 1 C for long-term cycling performance. In the cell using bare Li foil, the discharge/charge capacity starts fading after 100 cycles, decreasing to about 30 mAh g^{-1} after 200 cycles. However, using Li@200LiAlOx-ex as the anode, the cell maintains an extremely stable capacity of ~ 120 mAh g^{-1} after 450 cycles.

To further prove the concept, the Na-Na symmetrical cells were assembled to evaluate the Na plating/stripping behavior. **Fig. 2(e)** presents the electrochemical performances of the bare Na foil and Na@200$NaAlO_x$ in the symmetrical cells under the condition of 1 mA cm^{-2}/1 mAh cm^{-2}. The initial over-potential of bare Na foil is approximately 20 mV (versus Na^+/Na) and rapidly increases to over 40 mV (versus Na^+/Na) after ~ 200 h. After about 280 h, a sudden drop of the overpotential is observed, indicating the short circuit occurs for the bare Na. Very promisingly, for the Na@200$NaAlO_x$, the cell is stably running for over 1000 h with the low overpotential of 20 mV. When increasing the current density to 3 mA cm^{-2}, the overpotential of the bare Na increases dramatically up to 150 mV after only 100 h and a short circuit occurs shortly thereafter, as shown in **Fig. 2(f)**. For the Na@200$NaAlO_x$, even at the higher current density of 3 mA cm^{-2}, the overpotential is extremely stable over 1200 h without any short circuit. The electrochemical performances for both Li and Na metal anodes demonstrate that the $LiAlO_x$/$NaAlO_x$ coating can effectively improve the stability of Li/Na metal anode in different systems and shows potential for use in next-generation Li/Na-metal batteries. Particularly, $LiAlO_x$ coating derived from the two-step process indicates the unique properties and best performances compared to the Al_2O_3 and $LiAlO_x$ deposited directly at high temperatures. It is further proof that this approach is universal to be extended to different alkali metal anodes.

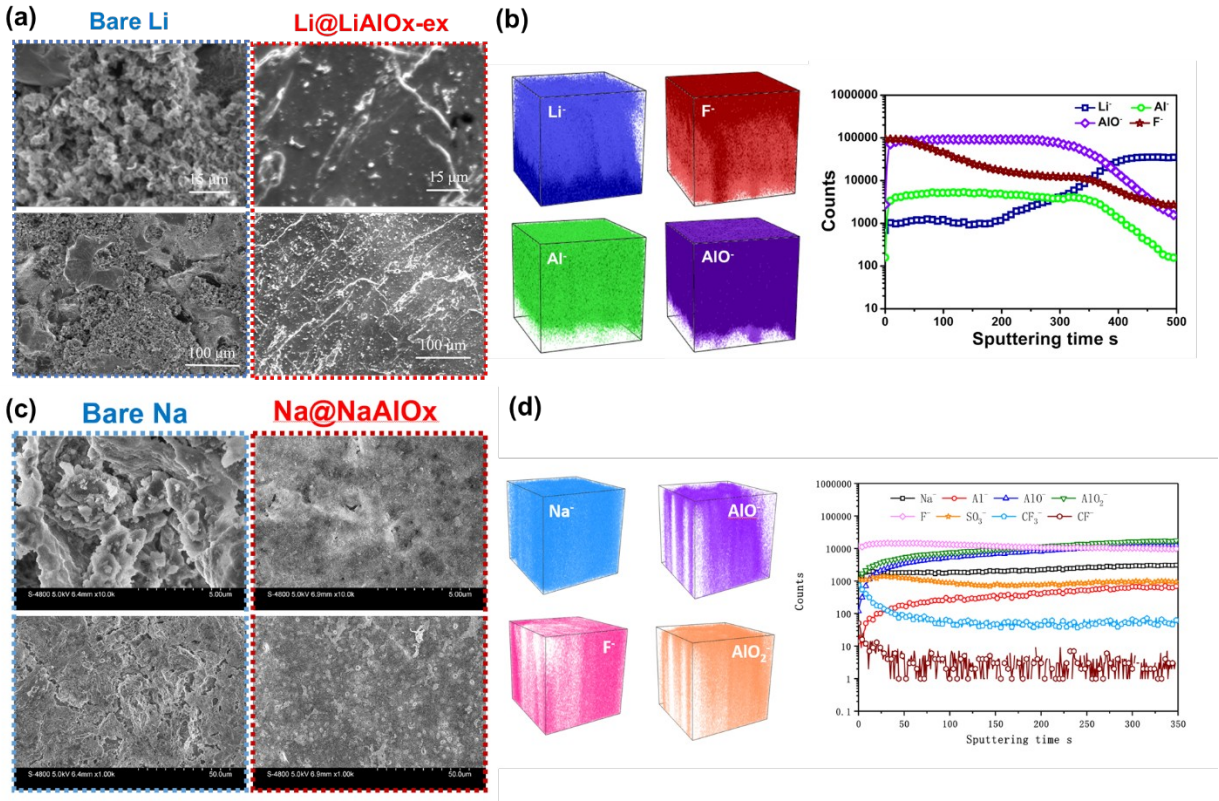

Fig.3 Top-view SEM images of (a) bare Li foil and Li@200LiAlOx-ex after electrochemical cycling (50 cycles) ; (b) TOF-SIMS depth profiles and corresponding 3D reconstructed images of Li@200LiAlOx-ex after electrochemical cycling. Top-view SEM images of (c) bare Na foil and Na@200NaAlOx after electrochemical cycling (50 cycles) ; (d) TOF-SIMS depth profiles and corresponding 3D reconstructed images of $Na@200NaAlO_x$ after electrochemical cycling.

.

To understand the influence of the $LiAlO_x$ layers on the Li deposition behavior, the morphology of Li metal was imaged after cycling by SEM. **Fig. S18** shows the SEM images of pristine Li foil after the different depths of electrochemical cycling (10 cycles, 20 cycles, and 30 cycles) at a current density of 1 mA cm^{-2} with a capacity limit of 1 mAh cm^{-2}. The mossy Li and dead Li layers are formed within 10 cycles, becoming more serious after deeper cycling. With 50 cycles of Li plating/stripping (**Fig.3 (a)**), a porous mossy structure with a rougher surface and obvious cracks are observed on the Li. These issues cause the increasing polarization of the cell and finally the short circuit. In comparison, the morphologies of the Li@200LiAlOx-ex are

drastically different, as shown in **Fig. S19** and **Fig. 3 (a)**. With the different cycling stages (10 cycles, 20 cycles, and 30 cycles), as shown in **Fig.S19**, the surfaces and morphologies of the Li@200$LiAlO_x$-ex are almost no changes. After 50 cycles of Li plating/stripping, the Li dendrite growth and dead Li formation are effectively reduced with the $LiAlO_x$ coating, which leads to significantly enhanced electrochemical performances.

Besides the morphology, the chemical compositions of the SEI are another critical factor for the Li deposition behavior and electrochemical performances. To understand the compositional changes following the plating/stripping cycling experiments, TOF-SIMS measurements were carried out. **Fig. S20** presents the TOF-SIMS results (including surface chemical ion images, depth profiles and corresponding 3D reconstructed images) of bare Li foil after plating/stripping cycling experiments at a current density of 1 mA cm^{-2} with a capacity limit of 1 mAh cm^{-2}. The bare Li shows significant penetration of F from electrolyte with a long sputtering time (over 500 s), which is related to the thick dead Li layer formation. However, as shown in **Fig. 3(b)** and **Fig. S21**, the $LiAlO_x$ coating remains on the top surface and with only slight changes compared to the spectra before cycling, in which the sputtering time is around 400 s. From the TOF-SIMS analysis of the SEI, it is found that the LiAlOx coating is robust and chemical/electrochemical stable during the Li plating/stripping process. To have a better understanding and comparison of the SEI, the XASNES at Al K-edge were performed for Li@200Al_2O_3, Li@200$LiAlO_x$-in, and Li@200$LiAlO_x$-ex after cycling. After cycling, the XASNES spectra of Al K-edge (**Fig.S22**) become broader, with peak a shift to higher energy compared to that of before cycling. Moreover, the intensities of spectra for Li@200Al_2O_3 and Li@200$LiAlO_x$-in dramatically decrease compared to that of Li@200$LiAlO_x$-ex, indicating the degradation of the coating layers during cycling. It further confirms that Li@200$LiAlO_x$-ex is the most stable protective layer during cycling.

Similarly, the surface morphology and composition for bare Na and Na@200$NaAlO_x$ after electrochemical cycling were further investigated. **Fig. 3 (c)** shows the top view SEM images of bare Na and Na@200$NaAlO_x$ after cycling. For the bare Na, the mossy Na is formed after the cycling, and the surface of the Na becomes rough with cracks. Remarkably, the surface of the Na@200$NaAlO_x$ after cycling is much smoother without any dendritic and mossy Na formation, which is one of the reasons for the significantly enhanced electrochemical performances. The

chemical composition of the interface was studied by TOF-SIMS, as shown in **Fig. S23** and **Fig. 3 (d)**. For the bare Na after cycling, strong signals of F^-, CF_3^-, SO_3^- secondary ion species are observed, demonstrating the decomposition of the electrolyte components as well as the thick dead Na layer growth. As a comparison, the AlO^- and AlO_2^- secondary ion species from the $NaAlO_x$ layer remain with minor changes, indicating that the NaAlOx protective layer is extremely stable during the electrochemical cycling, consistent with the results of electrochemical performances.

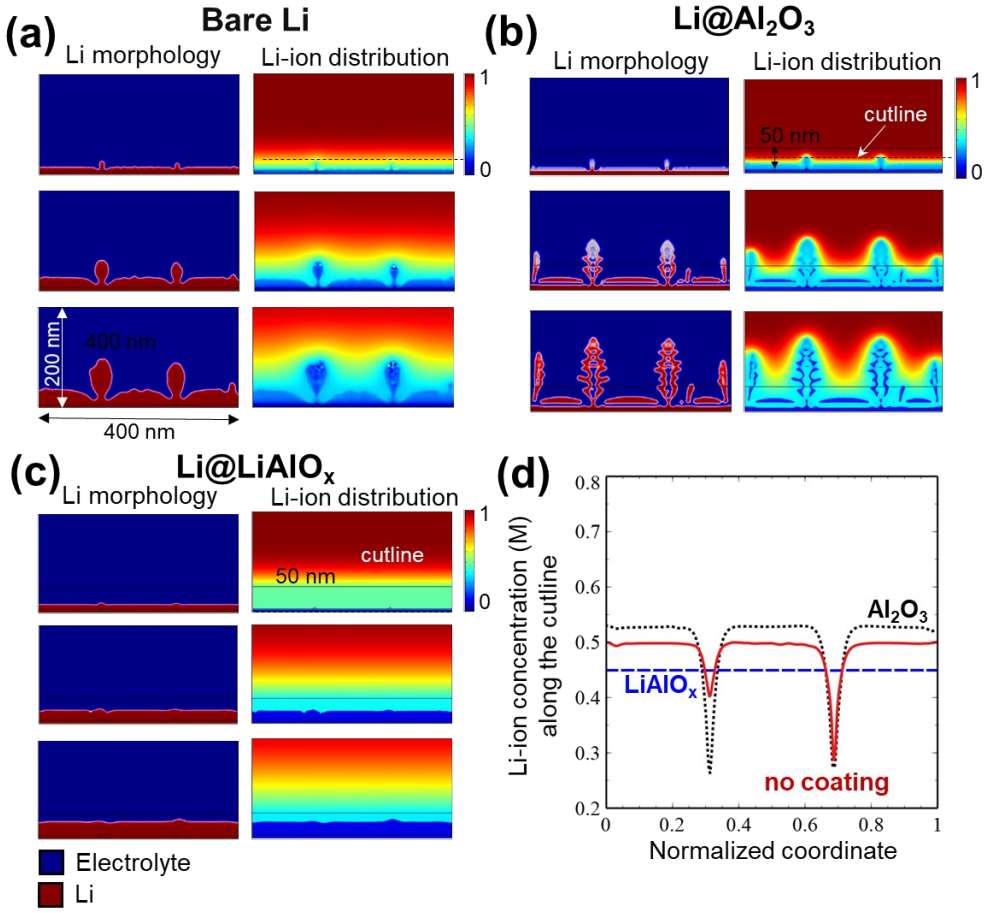

Fig.4 The morphological evolution of deposits Li and the distribution of Li-ion concentration under different coatings: (a) bare Li, (b) Li@Al_2O_3, and (c) Li@$LiAlO_x$. (d) The plot of Li-ion concentration near the interface at the beginning of the Li deposition process, showing the high ionic diffusitivity layer is beneficial for homogenizing the Li-ion distribution, which is a key driving force for uniform Li deposition.

To confirm the benefit of highly ionic conductive coating layer, the electrochemical phase-field model was performed. The approximated Li-ion diffusion coefficient of each coating used in this study are as follows: $LiAlO_x$ (1.4×10^{-11} m^2s^{-1}) >> uncoated surface (4.6×10^{-13} m^2s^{-1}) > Al_2O_3 (1.0×10^{-13} m^2s^{-1})[31-32]. **Fig.4 (a)-(c)** illustrate the simulated spatiotemporal evolution of deposits Li and the associated Li-ion distribution during Li plating under different coating conditions. Despite the same initial surface morphology for all studies, in which two small Li perturbations are introduced, Li@$LiAlO_x$ shows the surface of deposits Li remains uniform throughout the Li plating process, which is consistent with the experimental characterization that no dendrite after cycling is observed under the $LiAlO_x$ coating (**Fig.3 (a)** or **Fig. S19**). This is thanks to the intrinsic nature of the highly ionic conductive layer. Once Li-ions are reduced to Li atoms by the charge transfer reaction at the electrode surface, Li-ions in the coating layer (or electrolyte) quickly diffuse to the interface to replace the depleted Li-ions. Thus, the homogeneous distribution of Li-ions along the interface is well-maintained. On the other hand, when Li-ion diffusion near the interface is slow, bare Li as an example, the gradient of Li-ion concentration closed to the interface is evident, as shown in **Fig.4 (d)**. The variation of Li-ion concentration along the interface contributes to the nonuniform driving force for Li electrodeposition, thus resulting in the dendritic morphology of Li. The results agree with the experimental observation in **Fig.3 (a)** or **Fig. S18**, showing porous mossy Li structure after cycling. Moreover, for Li@Al_2O_3, whose coating layer is considered thick and highly non-ionic conductive, the Li dendrite quickly grows due to the significant Li-ion concentration gradient, substantially deteriorating cyclic performance (**Fig. S14**).

Conclusion

In conclusion, we successfully develop a universal approach to deposit ionic conductive interfaces for the alkali metal anodes by ALD. In the unique two-step ALD process, there is no Li/Na precursor required during deposition and Li/Na metal plays the role of Li/Na source. The $LiAlO_x$/$NaAlO_x$ coatings derived by a two-step strategy are uniform, smooth, and highly controllable. The ionic conductive coating layers can significantly improve the electrochemical performances of the Li and Na metal anodes in symmetric cells and full cells. Multiple evidence reveals that the ionic conductive coatings are chemically and electrochemically stable during

electrochemical plating/stripping and can reduce the Li/Na dendrite growth and dead Li/Na layer formation, resulting in performance improvement. We further investigate the influence of the ALD deposition temperatures on the Li metal anode's morphology, composition, and performance. Although the $LiAlO_x$ is also directly achieved with a high-temperature ALD process (Li@nLiAlOx-in), the surface of Li metal turns rough and corroded when the deposition temperature is above the melting point. We believe that this work can not only open a new window on creating ionic conductive layers on alkali metal without alkali precursor but also provides new insight into the temperature effects during the ALD deposition process when using temperature-sensitive alkali metal as a substrate.

Acknowledgments

This research was supported by the Natural Science and Engineering Research Council of Canada (NSERC), the Canada Foundation for Innovation (CFI), and the University of Western Ontario (UWO). We gratefully acknowledge Dr. Heng-Yong Nie for his help in the discussion on TOF-SIMS results. We would like to acknowledge the technical expertise of Mr. Jack Hendriks at the Western Tandetron Accelerator Facility. This research used resources of the Advanced Light Source, a DOE Office of Science User Facility under contract no. DE-AC02-05CH11231.

References

1. Cheng, X. B.; Zhang, R.; Zhao, C. Z.; Zhang, Q., Toward Safe Lithium Metal Anode in Rechargeable Batteries: A Review. *Chem. Rev.* **2017,** *117* (15), 10403-10473.
2. Lin, D.; Liu, Y.; Cui, Y., Reviving the lithium metal anode for high-energy batteries. *Nat Nanotechnol* **2017,** *12* (3), 194-206.
3. Zhao, Y.; Adair, K. R.; Sun, X., Recent developments and insights into the understanding of Na metal anodes for Na-metal batteries. *Energy & Environmental Science* **2018,** *11* (10), 2673-2695.
4. Lou, S.; Zhang, F.; Fu, C.; Chen, M.; Ma, Y.; Yin, G.; Wang, J., Interface Issues and Challenges in All-Solid-State Batteries: Lithium, Sodium, and Beyond. *Adv. Mater.* **2021,** *33* (6), e2000721.
5. Lei, Y.-J.; Yan, Z.-C.; Lai, W.-H.; Chou, S.-L.; Wang, Y.-X.; Liu, H.-K.; Dou, S.-X., Tailoring MXene-Based Materials for Sodium-Ion Storage: Synthesis, Mechanisms, and Applications. *Electrochemical Energy Reviews* **2020,** *3* (4), 766-792.

6. Wang, H.; Liu, Y.; Li, Y.; Cui, Y., Lithium Metal Anode Materials Design: Interphase and Host. *Electrochemical Energy Reviews* **2019,** *2* (4), 509-517.
7. Zhang, X.; Yang, Y.; Zhou, Z., Towards practical lithium-metal anodes. *Chem. Soc. Rev.* **2020,** *49* (10), 3040-3071.
8. Xu, R.; Cheng, X.-B.; Yan, C.; Zhang, X.-Q.; Xiao, Y.; Zhao, C.-Z.; Huang, J.-Q.; Zhang, Q., Artificial Interphases for Highly Stable Lithium Metal Anode. *Matter* **2019,** *1* (2), 317-344.
9. Luo, Z.; Qiu, X.; Liu, C.; Li, S.; Wang, C.; Zou, G.; Hou, H.; Ji, X., Interfacial challenges towards stable Li metal anode. *Nano Energy* **2021,** *79*, 105507.
10. Han, Z.; Zhang, C.; Lin, Q.; Zhang, Y.; Deng, Y.; Han, J.; Wu, D.; Kang, F.; Yang, Q. H.; Lv, W., A Protective Layer for Lithium Metal Anode: Why and How. *Small Methods* **2021,** *5* (4), e2001035.
11. Chu, Y.; Shen, Y.; Guo, F.; Zhao, X.; Dong, Q.; Zhang, Q.; Li, W.; Chen, H.; Luo, Z.; Chen, L., Advanced Characterizations of Solid Electrolyte Interphases in Lithium-Ion Batteries. *Electrochemical Energy Reviews* **2019,** *3* (1), 187-219.
12. Wang, G.; Chen, C.; Chen, Y.; Kang, X.; Yang, C.; Wang, F.; Liu, Y.; Xiong, X., Self-Stabilized and Strongly Adhesive Supramolecular Polymer Protective Layer Enables Ultrahigh-Rate and Large-Capacity Lithium-Metal Anode. *Angew. Chem. Int. Ed. Engl.* **2020,** *59* (5), 2055-2060.
13. Liu, D. H.; Bai, Z.; Li, M.; Yu, A.; Luo, D.; Liu, W.; Yang, L.; Lu, J.; Amine, K.; Chen, Z., Developing high safety Li-metal anodes for future high-energy Li-metal batteries: strategies and perspectives. *Chem. Soc. Rev.* **2020,** *49* (15), 5407-5445.
14. Gao, Y.; Yan, Z.; Gray, J. L.; He, X.; Wang, D.; Chen, T.; Huang, Q.; Li, Y. C.; Wang, H.; Kim, S. H.; Mallouk, T. E.; Wang, D., Polymer-inorganic solid-electrolyte interphase for stable lithium metal batteries under lean electrolyte conditions. *Nat Mater* **2019,** *18* (4), 384-389.
15. Gao, Y.; Rojas, T.; Wang, K.; Liu, S.; Wang, D.; Chen, T.; Wang, H.; Ngo, A. T.; Wang, D., Low-temperature and high-rate-charging lithium metal batteries enabled by an electrochemically active monolayer-regulated interface. *Nature Energy* **2020,** *5* (7), 534-542.
16. Xie, J.; Liao, L.; Gong, Y.; Li, Y.; Shi, F.; Pei, A.; Sun, J.; Zhang, R.; Kong, B.; Subbaraman, R.; Christensen, J.; Cui, Y., Stitching h-BN by atomic layer deposition of LiF as a stable interface for lithium metal anode. *Science Advances* **2017,** *3*, eaao3170.
17. Wu, J.; Rao, Z.; Liu, X.; Shen, Y.; Fang, C.; Yuan, L.; Li, Z.; Zhang, W.; Xie, X.; Huang, Y., Polycationic Polymer Layer for Air-Stable and Dendrite-Free Li Metal Anodes in Carbonate Electrolytes. *Adv. Mater.* **2021,** *33* (12), e2007428.
18. Lin, X.-D.; Gu, Y.; Shen, X.-R.; Wang, W.-W.; Hong, Y.-H.; Wu, Q.-H.; Zhou, Z.-Y.; Wu, D.-Y.; Chang, J.-K.; Zheng, M.-S.; Mao, B.-W.; Dong, Q.-F., An oxygen-blocking oriented multifunctional solid–electrolyte interphase as a protective layer for a lithium metal anode in lithium–oxygen batteries. *Energy & Environmental Science* **2021,** *14* (3), 1439-1448.
19. Xiao, J.; Zhai, P.; Wei, Y.; Zhang, X.; Yang, W.; Cui, S.; Jin, C.; Liu, W.; Wang, X.; Jiang, H.; Luo, Z.; Zhang, X.; Gong, Y., In-Situ Formed Protecting Layer from Organic/Inorganic Concrete for Dendrite-Free Lithium Metal Anodes. *Nano Lett.* **2020,** *20* (5), 3911-3917.

20. Zhao, Y.; Zhang, L.; Liu, J.; Adair, K.; Zhao, F.; Sun, Y.; Wu, T.; Bi, X.; Amine, K.; Lu, J.; Sun, X., Atomic/molecular layer deposition for energy storage and conversion. *Chem. Soc. Rev.* **2021,** *50* (6), 3889-3956.
21. Zhao, Y.; Zheng, K.; Sun, X., Addressing Interfacial Issues in Liquid-Based and Solid-State Batteries by Atomic and Molecular Layer Deposition. *Joule* **2018,** *2* (12), 2583-2604.
22. Zhang, R.; Li, Y.; Qiao, L.; Li, D.; Deng, J.; Zhou, J.; Xie, L.; Hou, Y.; Wang, T.; Tian, W.; Cao, J.; Cheng, F.; Yang, B.; Liang, K.; Chen, P.; Kong, B., Atomic layer deposition assisted superassembly of ultrathin ZnO layer decorated hierarchical Cu foam for stable lithium metal anode. *Energy Storage Materials* **2021,** *37*, 123-134.
23. Sun, Y.; Zhao, C.; Adair, K. R.; Zhao, Y.; Goncharova, L. V.; Liang, J.; Wang, C.; Li, J.; Li, R.; Cai, M.; Sham, T.-K.; Sun, X., Regulated lithium plating and stripping by a nano-scale gradient inorganic–organic coating for stable lithium metal anodes. *Energy & Environmental Science* **2021,** *14* (7), 4085-4094.
24. Oyakhire, S. T.; Huang, W.; Wang, H.; Boyle, D. T.; Schneider, J. R.; Paula, C.; Wu, Y.; Cui, Y.; Bent, S. F., Revealing and Elucidating ALD-Derived Control of Lithium Plating Microstructure. *Advanced Energy Materials* **2020,** *10* (44), 2002736.
25. Sun, Y.; Amirmaleki, M.; Zhao, Y.; Zhao, C.; Liang, J.; Wang, C.; Adair, K. R.; Li, J.; Cui, T.; Wang, G.; Li, R.; Filleter, T.; Cai, M.; Sham, T. K.; Sun, X., Tailoring the Mechanical and Electrochemical Properties of an Artificial Interphase for High-Performance Metallic Lithium Anode. *Advanced Energy Materials* **2020,** *10* (28), 2001139.
26. Zhao, Y.; Goncharova, L. V.; Lushington, A.; Sun, Q.; Yadegari, H.; Wang, B.; Xiao, W.; Li, R.; Sun, X., Superior Stable and Long Life Sodium Metal Anodes Achieved by Atomic Layer Deposition. *Adv. Mater.* **2017,** *29* (18).
27. Zhao, Y.; Goncharova, L. V.; Zhang, Q.; Kaghazchi, P.; Sun, Q.; Lushington, A.; Wang, B.; Li, R.; Sun, X., Inorganic-Organic Coating via Molecular Layer Deposition Enables Long Life Sodium Metal Anode. *Nano Lett.* **2017,** *17* (9), 5653-5659.
28. Zhang, S.; Zhao, Y.; Zhao, F.; Zhang, L.; Wang, C.; Li, X.; Liang, J.; Li, W.; Sun, Q.; Yu, C.; Luo, J.; Doyle-Davis, K.; Li, R.; Sham, T. K.; Sun, X., Gradiently Sodiated Alucone as an Interfacial Stabilizing Strategy for Solid-State Na Metal Batteries. *Adv. Funct. Mater.* **2020,** *30* (22), 2001118.
29. Liu, J.; Banis, M. N.; Xiao, B.; Sun, Q.; Lushington, A.; Li, R.; Guo, J.; Sham, T.-K.; Sun, X., Atomically precise growth of sodium titanates as anode materials for high-rate and ultralong cycle-life sodium-ion batteries. *J. Mater. Chem. A* **2015,** *3* (48), 24281-24288.
30. Wang, B.; Zhao, Y.; Banis, M. N.; Sun, Q.; Adair, K. R.; Li, R.; Sham, T. K.; Sun, X., Atomic Layer Deposition of Lithium Niobium Oxides as Potential Solid-State Electrolytes for Lithium-Ion Batteries. *ACS Appl Mater Interfaces* **2018,** *10* (2), 1654-1661.
31. Huang, B.; Zhao, Z.; Sun, Y.; Wang, M.; Chen, L.; Gu, Y., Lithium-ion conductor LiAlO2 coated LiNi0.8Mn0.1Co0.1O2 as cathode material for lithium-ion batteries. *Solid State Ionics* **2019,** *338*, 31-38.
32. Jung, S. C.; Kim, H. J.; Choi, J. W.; Han, Y. K., Sodium ion diffusion in Al2O3: a distinct perspective compared with lithium ion diffusion. *Nano Lett.* **2014,** *14* (11), 6559-63.